Journal of the Earth and Space Physics
Homepage: https://jesphys.ut.ac.ir
Vol. 51, No. 4, Winter 2026, P. 133-152
(Research Article)

Dry Lightning Contributing to Wildfires in the Zagros Forested Area: A Meteorological and Environmental Analysis of Extreme Events in June 2019 and May 2020

Khansalari, S.[1] ✉ | Fazel-Rastgar, F.[2] | Guehaz, R.[2,3] | Sivakumar, V.[4]

1. Atmospheric Science and Meteorological Research Center, Tehran, Iran.
2. Department of Physics, School of Chemistry and Physics, University of KwaZulu-Natal, Durban 4000, South Africa.
3. Center for the Development of Advanced Technologies (CDTA), Algiers, Algeria.
4. S. V. Raman Researchers Roadmap, Westville, Durban 4000, South Africa.

Corresponding Author E-mail: khansalari@yahoo.com

(Received: 27 April 2025, Revised: 1 June 2025, Accepted: 2 Aug 2025, Published online: 17 March 2026)

Abstract

Wildfires in forested and pasture areas of Iran have increased in recent years, raising concerns about their ignition sources and environmental drivers. Among natural causes, lightning—particularly dry lightning—plays a significant role in initiating wildfires under specific meteorological conditions. This study aims to analyze the contribution of dry lightning to major wildfire events in Iran's Zagros region during May 2020 and June 2019. To achieve this, we utilized a combination of satellite-based fire data from FIRMS and lightning data from the Earth Networks Total Lightning Network (ENTLN). In addition, meteorological datasets and reanalysis models were employed to assess drought conditions and fire-conducive weather patterns. Key indices such as the Fire Weather Index (FWI), Fire Danger Index (FDI), Burned Area Index (BI), Keetch–Byram Drought Index (KBDI), and the Standardized Precipitation Evaporation Index (SPEI) were applied. Burn severity was evaluated using Landsat-8 and Sentinel-2 imagery. Our results reveal a strong correlation between wildfire activity and lightning occurrences, particularly in areas with dry vegetation, elevated temperatures, and minimal precipitation. Quantitative validation during two major fire events—June 2019 and May 2020—confirms that wildfires were most intense on days when dry lightning coincided with elevated Fire Weather Index (FWI) values. For instance, on June 6 and 7, 2019, 4332 and 4833 dry lightning strikes were recorded, with FWI values of 33.8 and 39.4, and over 900 high-confidence fire detections observed each day. Similarly, May 20 and 21, 2020 exhibited peaks in all three factors, with up to 5773 lightning strikes and FWI values exceeding 24. These findings substantiate the synergistic role of dry lightning and fuel flammability in wildfire ignition and highlight the importance of multi-variable monitoring for fire risk assessment. This study highlights the importance of integrating satellite data, lightning observations, and fire indices for wildfire risk assessment. Ultimately, this research provides valuable insight into the mechanisms of dry lightning-induced wildfires and contributes to developing early warning strategies and adaptation measures under changing climate conditions.

Keywords: Fire Indices, FIRMS, Forest wildfire, Lightning, Zagros Mountains.

1. Introduction

Climate change is a critical global challenge, evident through phenomena such as drought, land degradation, and altered precipitation patterns (Bitar et al., 2021). These climatic shifts have substantial ecological consequences, including increased lightning activity and a corresponding rise in wildfire occurrences (Song et al., 2024). Understanding the links between climate dynamics and wildfire behavior is essential for developing effective adaptation and mitigation strategies. Forest fires not only devastate ecosystems but also result in substantial economic and social consequences (Kala, 2023). The frequency and severity of wildfires have increased in recent years, often correlating with the effects of climate change (Williams et al., 2019). Wildfire-generated heat leads to updrafts that promote atmospheric instability. This rising humid air can form pyrocumulus clouds, which, under intense heat and favorable atmospheric conditions, may develop into pyrocumulonimbus clouds capable of producing dry lightning—lightning without significant precipitation. Such dry lightning can ignite new fires far from the original blaze, complicating containment efforts. Firestorms and intense winds further exacerbate fire spread. Dry

Cite this article: Khansalari, S., Fazel-Rastgar, F., Guehaz, R., & Sivakumar, V., (2026). Dry Lightning Contributing to Wildfires in the Zagros Forested Area: A Meteorological and Environmental Analysis of Extreme Events in June 2019 and May 2020. *Journal of the Earth and Space Physics*, 51(4), 133-152. DOI: http//doi.org/10.22059/jesphys.2025.393620.1007679

E-mail: (2) farah_rast@yahoo.com (2,3) rguehaz@cdta.dz (4) svsk74@protonmail.com

Publisher: University of Tehran Press.
DOI: http//doi.org/10.22059/jesphys.2025.393620.1007679
Print ISSN: 2538-371X
Online ISSN: 2538-3906

lightning is recognized as the most common natural cause of wildfires (Fuquay et al., 1972; Rakov et al., 1998; Rorig and Ferguson, 1999; Podur et al., 2003; Moris et al., 2020; Kalashnikov et al., 2023; Gao et al., 2024). Burned areas have been expanding in the Middle East and Southeast Asia by approximately 3–4% (Giglio et al., 2013). For instance, in Canada, over 8,000 wildfires occur annually, burning around 2.1–2.5 million hectares—approximately 85% of which are attributed to lightning, according to the National Forestry Database (de Morais, 2013). Fires can affect forests, shrublands, and grasslands and are typically ignited either by lightning or human negligence (Bryant, 2008). In addition to natural causes, strong seasonal winds—intensified by climate change—can spark fires by bringing down power lines or igniting dry fuels (Lee, 2005; Fazel-Rastgar and Sivakumar, 2022). The role of lightning in initiating wildfires is thus a central topic in environmental research. Thunderstorms that develop under favorable meteorological conditions can easily ignite flammable material (Moris et al., 2020; Jiao et al., 2023). Meteorological factors—such as temperature, wind speed, humidity, and drought—significantly influence the likelihood of wildfire ignition and spread (Barbero et al., 2018; Fazel-Rastgar and Sivakumar, 2022).

To assess wildfire risk, various indices such as the Fire Weather Index (FWI), Burned Area Index (BI), and Fire Danger Index (FDI) have been developed (Di Giuseppe et al., 2020; Pereira et al., 2020; Markos et al., 2023; Mohammadian Bishe et al., 2023). Recent statistical models (Song et al., 2024) suggest that lightning-induced fires are exacerbated by the abundance of dry fuels and increased lightning ignition efficiency—conditions increasingly common due to more frequent droughts and thunderstorms under a changing climate (Bowman et al., 2017). Without appropriate mitigation strategies, the incidence of lightning-induced wildfires is likely to rise further (Božičeк et al., 2023).

In the Middle East, the extent of burned areas has significantly increased. For example, in Iraq, a country neighboring Iran, burned areas expanded by an average of 71.7 km² per year from 2001 to 2019, with 29% of the total burning concentrated in Ninawa Governorate (Rahimi et al., 2024). In Iran, forest fires—particularly in the Zagros and Alborz ranges—are increasingly becoming critical environmental hazards. Despite their significance, the role of climate and weather conditions in influencing wildfire susceptibility in Iran remains underexplored (Jaafari et al., 2018). The Zagros Forests are the largest expanse of broadleaf woodlands in Iran, covering over 5 million hectares and stretching from the northwest to the southeast. These forests are predominantly composed of Quercus brantii (Persian oak), which accounts for more than 70% of the tree population (FAO, 2005). Other native species include *Pistacia atlantica*, Amygdalus scoparia, Crataegus spp., and Celtis caucasica. Spatial heterogeneity is a key feature of the Zagros landscape: the western slopes receive greater precipitation and support denser and more continuous forest cover, while the eastern slopes are characterized by semi-arid conditions and fragmented woodland. This ecological gradient influences fire susceptibility and fuel availability. Surface vegetation patterns derived from Sentinel-2 and Landsat imagery confirm this spatial variability, with visible contrasts in land cover and canopy density that affect fire behavior and detection. While various global studies have quantified the relative roles of lightning and anthropogenic activity in wildfire ignition, similar efforts remain lacking in Iran. For instance, Janssen et al. (2023) demonstrated that lightning is responsible for approximately 77% of the burned area in extratropical intact forests worldwide and that climate warming may significantly increase lightning occurrence in such regions. However, no region-specific studies currently exist for the Zagros Mountains or broader Iranian forests, despite growing evidence that dry lightning could become a more dominant ignition source under changing climate conditions. This study serves as a preliminary effort to address this gap by examining two lightning-driven wildfire events in southwestern Iran.

In Iran, forest fires impose significant economic costs, estimated at approximately US $13,000 per hectare (Tehran Times, 2019). For example, in May 2020, fires in the Zagros Mountains destroyed over 4.7 million hectares of natural resources in Khuzestan Province—an area with one of the largest forest zones in the region. These fires

extended across at least seven provinces, damaging ecosystems and biodiversity. Previous studies have explored various wildfire drivers, including vegetation characteristics, topography, and human activities. In parallel, they have recommended preventive strategies such as early warning systems, fire suppression techniques, and post-fire recovery plans (Jahdi et al., 2015; Jaafari et al., 2017; Jaafari et al., 2018).

The main objective of this study is to investigate the role of dry thunderstorms as a major ignition source of recent forest fires in the Zagros Mountains. This research also seeks to propose climate adaptation measures for fire risk reduction and to assess the effectiveness of satellite-based tools such as Landsat-8 and Sentinel-2 for burn severity detection. To the best of our knowledge, this study is the first to provide a regional-scale spatiotemporal assessment of dry lightning-induced wildfires in Iran's Zagros region, using an integrated dataset combining satellite-derived fire observations (FIRMS), lightning data (ENTLN), and multiple fire indices (FWI, FDI, BI, and KBDI). This multifaceted approach addresses a critical gap in existing wildfire research in Iran, particularly regarding the quantitative linkage between atmospheric triggers and fire ignition under arid climatic conditions. Based on comparative evaluations, Landsat's Thematic Mapper sensor is found to be the most suitable for this application (Keeley, 2009).

2. Material and Methods

2-1. Study Area

This study focuses on a significant wildfire event in Iran, specifically the Khaeez Protected Area, situated between Kohgiluyeh and Boyer-Ahmad and Khuzestan provinces, as shown in Figure 1. This region lies within the heart of the Zagros range, one of the most significant and extensive mountain systems in the Middle East, playing a critical role in the country's climatic balance and biodiversity. The Zagros Mountains, stretching approximately 1,600 kilometers, form the western edge of the Iranian Plateau. The forests in this region are predominantly composed of Persian oak (Quercus Brantii) and cover nearly six million hectares across 11 provinces—accounting for about 40% of Iran's total forest area (Sagheb-Talebi et al., 2014).

In recent years, widespread and recurrent wildfires have increasingly threatened these forests. Rising temperatures, prolonged droughts, land use changes, and weaknesses in fire management systems have been among the primary contributing factors. Overgrazing, agricultural expansion, and pest outbreaks have further reduced the natural regeneration capacity of these ecosystems, particularly during the hot and dry seasons of spring and summer. Among the most vulnerable areas is the Khaeez Protected Region, which covers approximately 33,000 hectares. This area has been under formal protection by Iran's Department of Environment since the early 2000s and is home to a rich variety of plant and animal species. Extensive wildfires in 2019 and 2020 affected over 1,700 hectares of this region, causing severe ecological damage (Jaafari et al., 2018).

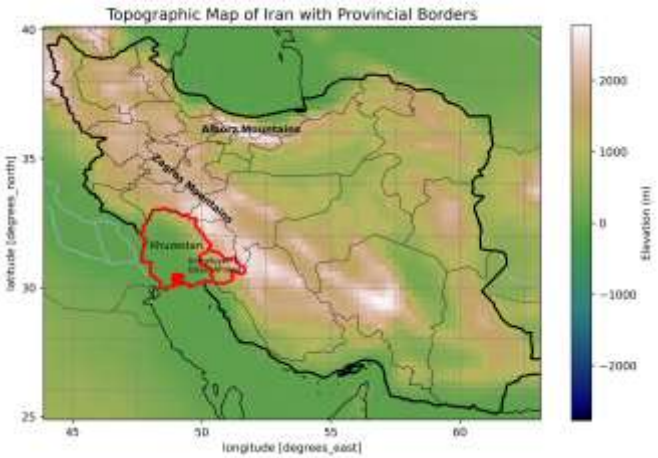

Figure 1. Topographic map of Iran showing the Zagros Mountains and the southwestern provinces of Khuzestan and Kohgiluyeh and Boyer-Ahmad within the study area.

2-2. Data

This study utilizes various meteorological datasets and reanalysis models, including data from the National Centers for Environmental Prediction (NCEP), the National Center for Atmospheric Research (NCAR), and NASA's Modern-Era Retrospective Analysis for Research and Applications (MERRA) model (Rienecker et al., 2011). In addition, hourly ERA5 reanalysis data from the European Centre for Medium-Range Weather Forecasts (ECMWF) were analyzed (Hersbach et al., 2020). To assess drought conditions in the study area, the Standardized Precipitation Evaporation Index (SPEI) was obtained from the SPEI database (https://spei.csic.es/database.html).

2-2-1. Meteorological and Reanalysis Data

Meteorological background conditions in this study were derived using multiple reanalysis datasets. Atmospheric variables were obtained from the NCEP/NCAR and MERRA models, which provided the large-scale environmental context for fire occurrence. ERA5 reanalysis data from the ECMWF were used to analyze key weather parameters and to compute fire danger indices. In addition, the Standardized Precipitation Evapotranspiration Index (SPEI) was retrieved to evaluate temporal variations in drought severity across the study area.

ERA5 reanalysis data were used at a spatial resolution of 0.25° (~31 km) with daily temporal resolution to compute fire weather indices. NCEP/NCAR data were used at a 2.5° resolution, and MERRA data at ~0.5°. All meteorological datasets were temporally subset to cover June 2019 and May 2020. For spatial consistency, data were clipped to the southern Zagros region (30°–33.5° N, 42.5°–52° E). Fire indices such as FWI, BI, FDI, and KBDI were computed using meteorological parameters from ERA5.

2-2-2. Satellite-Based Remote Sensing Data

To investigate forest fires and their relationship with lightning activity in the southern Zagros region, this study employed active fire data from NASA's Fire Information for Resource Management System (FIRMS). FIRMS provides near-real-time fire detection using data from the Moderate Resolution Imaging Spectroradiometer (MODIS) and the Visible Infrared Imaging Radiometer Suite (VIIRS). Since FIRMS provides full coverage of Iran, it is a reliable source for assessing fire dynamics in the study region.

The VIIRS fire layer, derived from the NASA/NOAA Suomi National Polar-orbiting Partnership (S-NPP), NOAA-20 (JPSS-1), and NOAA-21 (JPSS-2) satellites, delivers high-resolution information on active fire detection and thermal anomalies. These data enable the identification of persistent hotspots, spatial and temporal patterns of fire activity, and sources of thermal pollution such as gas flares or volcanic activity. VIIRS, which complements MODIS in producing global fire datasets, provides 375-meter resolution I-band data. This improved spatial resolution enhances detection of smaller fires and improves perimeter mapping for large fire events. VIIRS also offers superior nighttime detection performance, making it particularly valuable for real-time alert systems and detailed fire analysis. The VIIRS Fire and Thermal Anomalies product, with a sensor resolution of 375 meters and imagery resolution of 250 meters, is available twice daily. Red dots in the data represent the center of each 375-meter pixel exhibiting thermal anomalies. Polar-orbiting satellites allow for 3–4 daily observations over mid-latitudes, ensuring comprehensive monitoring. This study utilizes forest fire detections from VIIRS (https://firms.modaps.eosdis.nasa.gov/map).

Additionally, this study utilized Landsat 8 surface reflectance data from the LANDSAT/LC08/C01/T1_SR product via Google Earth Engine (GEE). These data are widely applied in agriculture, forestry, and environmental studies. Complementary imagery from Sentinel-2 (COPERNICUS/S2 Level-2) with a five-day revisit interval was also used to enhance analysis through GEE's cloud platform.

VIIRS fire data were filtered to retain only high-confidence fire pixels (confidence = "h"), and detections outside the defined Zagros region were excluded. For Landsat-8 and Sentinel-2 imagery, cloud masks (such as pixel_qa and QA60 bands) were applied in Google Earth Engine to exclude cloudy observations. Burn severity was assessed

using the Normalized Burn Ratio (NBR) and the differenced NBR (dNBR) metrics, calculated across pre- and post-fire images.

2-2-3. Lightning Data

Lightning strike data, specifically cloud-to-ground (CG) strikes, were obtained from the Earth Networks Total Lightning Network (ENTLN). ENTLN consists of over 1,600 broadband sensors deployed across more than 40 countries. The system utilizes advanced Time-of-Arrival (TOA) techniques for accurate geolocation and time stamping of both intra-cloud (IC) and cloud-to-ground (CG) lightning discharges. ENTLN's multi-parameter algorithms allow for robust differentiation between IC and CG pulses, and the network has been widely used in studies on convective storms, lightning rates, storm tracking, and early warning systems. Recent studies have confirmed the system's spatial and temporal reliability and high detection efficiency (Thompson et al., 2014; Rudlosky, 2015; Bui et al., 2015; Lapierre et al., 2019; Zou et al., 2022). The network typically provides sub-minute temporal resolution and spatial accuracy ranging from 1 to 5 km, depending on proximity to sensors and terrain complexity.

For this study, only CG strikes were used. The lightning data were temporally filtered to match the two fire periods (June 2019 and May 2020) and spatially constrained to the Zagros Mountain region (30–33.5°N, 42.5–52°E). All timestamps were converted to Coordinated Universal Time (UTC) and synchronized with ERA5 meteorological data and VIIRS fire records from NASA FIRMS. Dry lightning events were defined as CG strikes occurring under Fire Weather Index (FWI) values greater than 30, following Wotton et al. (2010).

It is important to note that ENTLN does not have ground-based sensors within Iran. Instead, detections are interpolated from surrounding countries with higher lightning activity and denser sensor networks. As a result, detection accuracy may vary—especially in complex mountainous terrain such as the Zagros. Therefore, while ENTLN provides high spatiotemporal detail globally, its spatial resolution is not fixed and depends on regional sensor density and strike intensity. Although ENTLN generally provides high detection efficiency, its performance—like that of WWLLN—can be affected in mountainous or densely forested regions due to terrain-induced signal attenuation and limited ground sensor coverage. Several validation studies (e.g., Rudlosky, 2019; Bui et al., 2015; Zou et al., 2022) have reported spatial uncertainties of up to 5 km, which may increase further in complex topographies.

To enhance data transparency and accessibility, Table 1 summarizes the key datasets, parameters, and abbreviations used throughout the study.

Table 1. Summary of Datasets and Parameters.

Dataset	Source	Spatial Resolution	Temporal Resolution	Period	Parameters Used	Abbreviation
Meteorological Data	ERA5	0.25° (~31 km)	Daily	May 2020, June 2019	FWI, KBDI, FDI, BI	FWI, KBDI, etc.
Fire Data	Visible Infrared Imaging Radiometer Suite/ Fire Information for Resource Management System	~375 m	2–4 observations per day	May 2020, June 2019	Fire hotspots (confidence="h")	VIIRS/FIRMS
Satellite Imagery	Landsat-8, Sentinel-2	30 m, 10 m	16 days (Landsat), 5 days (Sentinel)	Pre/post fire	dNBR, NBR	-
Lightning Data	Earth Networks Total Lightning Network	Variable (~1–5 km, region-dependent)	Sub-minute (region-dependent detection latency)	May 2020, June 2019	CG strikes	ENTLN

2-3. Methods

Several fire indices to detect and analyze forest fire occurrences during major fire events in the study area were employed. By examining indices such as the Fire Weather Index (FWI), Fire Danger Index (FDI), Burning Index (BI), and Keetch–Byram Drought Index (KBDI), along with FIRMS active fire data, the study evaluates spatial and temporal fire patterns and explores their association with lightning strikes. This integrated approach enhances the understanding of fire dynamics and informs effective prevention strategies and policy development.

The Fire Weather Index (FWI) provides a numerical estimate of fire intensity based on meteorological conditions. It is widely recognized as a reliable indicator of fire danger, incorporating factors such as fuel availability (i.e., drought stress) and fire spread potential. Derived from the Canadian Fire Weather Index System, FWI combines variables that account for fuel moisture and wind speed, with higher values indicating increased fire risk. FWI data in this study are based on weather forcings from ECMWF's ERA5 and ERA-Interim reanalysis datasets (Hersbach et al., 2020; Vitolo et al., 2020).

To evaluate the role of dry lightning as a potential ignition mechanism for large-scale wildfires, a combined spatiotemporal analysis of lightning activity, Fire Weather Index (FWI) values, and confirmed wildfire occurrences was carried out. In this study, dry lightning was operationally defined as lightning strikes occurring under conditions where FWI exceeded 30, based on internationally recognized fire danger classifications (Wotton et al., 2010). For each day within the selected periods, regional mean FWI, the number of dry lightning events, and the count of high-confidence wildfires (confidence = “h”) derived from the VIIRS dataset were extracted. This integrative approach allowed for a systematic assessment of the compound fire risk arising from the interaction between ignition triggers and fuel flammability conditions.

The Burning Index (BI) estimates fire intensity by integrating the Spread Component and Energy Release Component. While BI is unitless, flame lengths are generally estimated to be approximately ten times the BI value, providing a practical metric for evaluating fire behavior and containment difficulty. The Keetch–Byram Drought Index (KBDI) assesses soil moisture levels within the top 8 inches of soil, with values ranging from 0 (fully saturated) to 800 (extreme drought stress). Although regionally calibrated, the KBDI provides consistent insight into drought-related fire potential across varied landscapes.

Fire indices such as FWI, FDI, BI, and KBDI (Podschwit et al., 2023) were used to assess fire risk in relation to environmental drivers, including air temperature, relative humidity, wind speed, soil moisture, and precipitation. Increased temperature and wind speed, along with reduced humidity and rainfall, generally elevate fire risk, as reflected in higher index values. These indices were derived from the ERA5 dataset, provided by ECMWF reanalysis through the Copernicus Emergency Management Service for the European Forest Fire Information System (EFFIS). ERA5, ECMWF’s fifth-generation reanalysis product, covers the global climate from 1940 to the present and is widely used in forest and rangeland fire studies (Podschwit et al., 2023).

3. Results and Discussion

3-1. Forest Fire Observations over Iran

Forest fires have become a significant environmental concern in Iran, affecting large areas of forests and rangelands. This section presents an analysis of fire events and the associated burned areas across Iran from 2001 to 2020, based on data from Iran Open Data (https://iranopendata.org/en/). Figure 2 illustrates the total number of fire events and the corresponding burned areas (in hectares) in forests and rangelands during this period. The analysis reveals a notable spike in forest destruction in 2020, with approximately 47,659 hectares affected. Between 2001 and 2020, fires destroyed an estimated total of 228,000 hectares of forests and rangelands in Iran, including 103,000 hectares of forests and 125,000 hectares of pastures. On average, over 9,000 hectares of forest and 11,000 hectares of rangeland were burned annually.

In 2020, the provinces with the highest levels of forest damage were primarily located in western and southwestern Iran, including Kurdistan, Qom, Fars, West Azerbaijan, and Kohgiluyeh and Boyer-Ahmad. These areas

are mainly situated within the forested zone of the Zagros Mountains. According to Iran Open Data, widespread fire outbreaks in the Zagros forest region were the primary cause of forest loss in 2020 and 2021, with an estimated 21,244 hectares affected over the two-year period. In comparison, 2019 recorded approximately 20,941 hectares of burned forest and rangeland. These statistics were drawn from Table 47659 on page 99 of the report titled Number of Fires and Consumed Rangelands and Forests 2001–2021, last updated on April 18, 2024 (https://iranopendata.org/en/).

3-2. Drought Situation and Forest Fires

Drought conditions in Iran have been a significant factor influencing the occurrence and intensity of wildfires in recent years. Figure 3 illustrates the Standardized Precipitation Evaporation Index (SPEI) over Iran for May (a) and June (b) during the wildfire events of 2019. Figures 3c and 3d show the SPEI for April (a month prior to the 2020 wildfire, highlighting potential dryness) and May 2020 (the period of the 2020 wildfire), respectively. The data were sourced from the SPEI website (https://spei.csic.es/database.html). Figures 3a and 3b reveal negative SPEI values (-1 to -3), indicating intense to extreme drought over the study area during the months leading up to and during the early June 6–7, 2019, wildfire events. However, an analysis of the SPEI for April 2019 (not shown here), two months prior to the June wildfire event, indicated near-normal values (greater than -0.5). It is important to note that heavy rainfall during the spring of 2019, which caused widespread flooding across Iran (Fazel-Rastgar, 2020), resulted in saturated wetlands and reservoirs. This precipitation triggered vegetation growth across vast areas, including the Zagros Forests and rangelands. However, the subsequent hot and dry conditions heightened the risk of wildfires, allowing them to spread rapidly. According to data published by the National Drought Warning and Monitoring Center, Iran's total precipitation increased significantly from 159.9 mm (from September 23, 2017, to September 23, 2018) to 310.2 mm during the corresponding period in 2019, representing a 94.9% increase. This total also surpassed the long-term average of 222.2 mm by approximately 39.6% (Tehran Times, 2019). The SPEI expands on the Standardized Precipitation Index (SPI) by incorporating both rainfall and potential evapotranspiration (PET) to assess drought conditions (Vicente-Serrano et al., 2010). The SPEI classification is as follows: no drought (SPEI greater than -0.5), mild drought (SPEI between -0.5 and -1), moderate drought (SPEI between -1.5 and -1), severe drought (SPEI between -2 and -1.5), and extreme drought (SPEI less than -2) (Paulo et al., 2012).

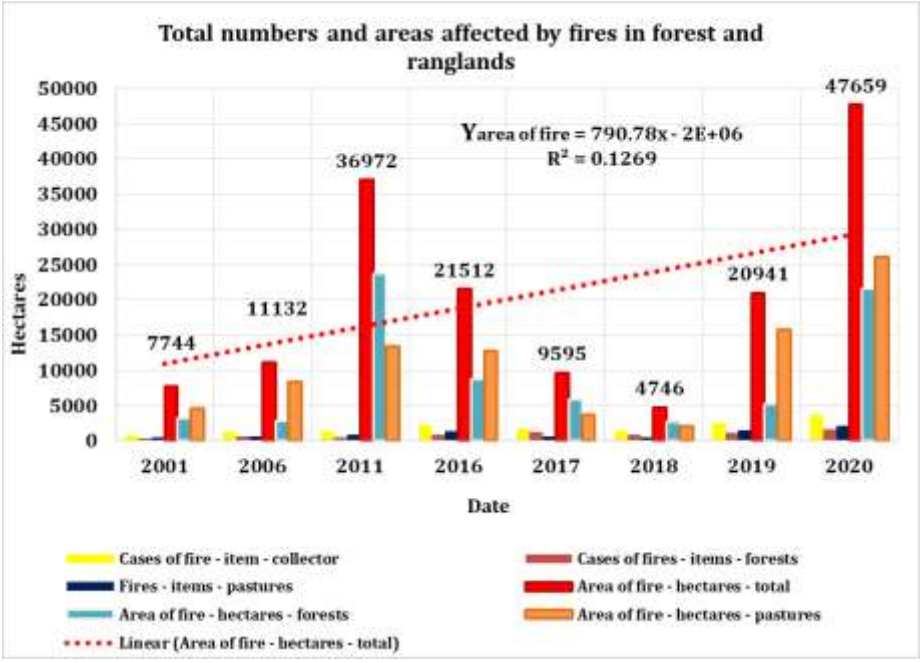

Figure 2. Total number of fire events and areas (in hectares) of forest and pasture destruction from 2001 to 2020. Data sourced from Iran Open Data.

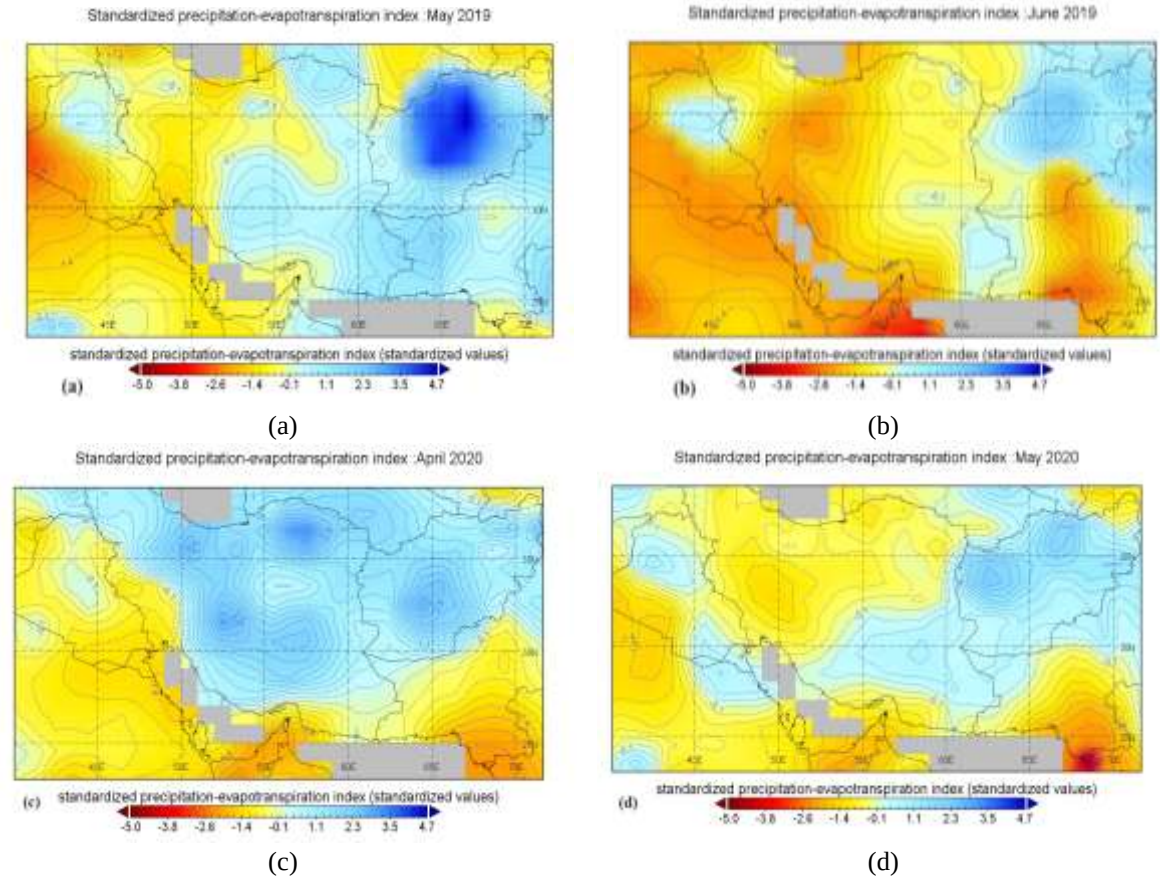

Figure 3. Standardized Precipitation Evaporation Index (SPEI) over the southern part of the study area: (a) May 2019, (b) June 2019, (c) April 2020, and (d) May 2020.

Figure 4 presents the monthly means from the NCEP datasets (Kalnay et al., 2018) for surface air temperatures (a) and precipitation rates (b) during May and June over the study area (latitude: 30°–35°; longitude: 47.5°–52.5°). The data reveal positive trends in air temperatures and negative trends in precipitation rates over recent decades. Higher temperatures contribute to increased atmospheric moisture, promoting conditions conducive to convective activity. Consequently, regions experiencing drought are more vulnerable to intense thunderstorms, often characterized by frequent lightning strikes (Janssen et al., 2023). Such weather conditions, as analyzed in this study, are particularly prevalent in the forested regions of the southern Zagros. Lightning, especially when accompanied by thunderstorms, poses a significant risk of igniting forest fires, particularly in areas with dry vegetation.

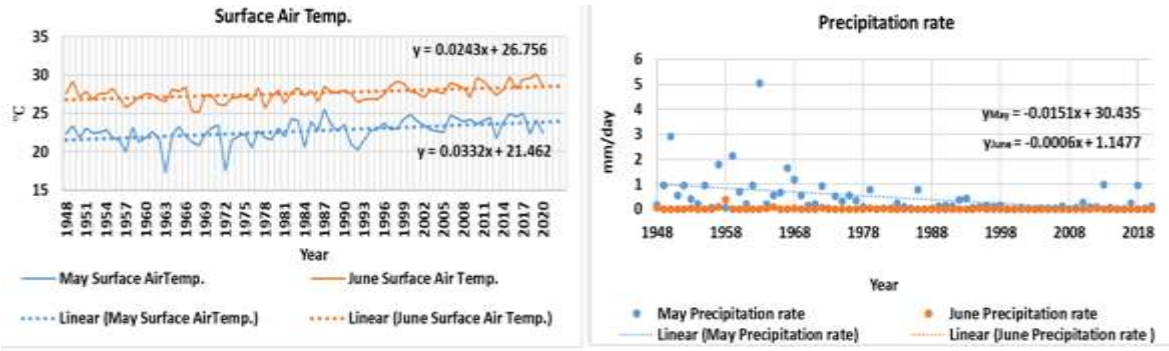

(a) (b)

Figure 4. Monthly means of (a) surface air temperature and (b) precipitation rate over the study area during May and June from 1948 to 2020.

3-3. The Burned Area Measured by the Landsat-8 and Sentinel-2 Satellites

This section presents a comparison of results obtained using two widely adopted spectral indices—the Normalized Burn Ratio (NBR) and the differenced NBR (dNBR)—for selected burned areas from several forest fires (Van Wagtendonk et al., 2004). The impacts of wildfires that occurred in May 2019 and June 2020 in the southern Zagros Forest region of Iran (Figure 5) are illustrated through burn severity maps derived from Landsat-8 (Figures 5a and 5c) and Sentinel-2 (Figures 5b and 5d) satellite imagery. These maps provide valuable insights into the spatial extent and intensity of the fire-affected areas.

Burn severity in this study was assessed using the differenced Normalized Burn Ratio (dNBR), calculated from pre- and post-fire imagery acquired by Landsat-8 and Sentinel-2. The classification of severity levels was conducted according to the thresholds proposed by Key and Benson (2006), which are widely adopted in post-fire impact studies. In this classification, very low dNBR values—ranging from approximately –0.500 to –0.251—represent areas of enhanced regrowth with high vigor, while values between –0.250 and –0.101 reflect low-level regrowth. Areas that experienced no discernible change due to fire fall between –0.100 and +0.099 and are considered unburned. As dNBR values increase beyond this neutral zone, burn severity rises accordingly. Low severity is typically associated with dNBR values from +0.100 to +0.269, moderate-low severity with values between +0.270 and +0.439, and moderate-high severity with values from +0.440 to +0.659. The most severe burn effects are represented by values greater than +0.660, extending up to approximately +1.300. These thresholds have been validated in various ecological assessments and provide a reliable basis for characterizing the impact of wildfires on vegetation cover and ecosystem structure.

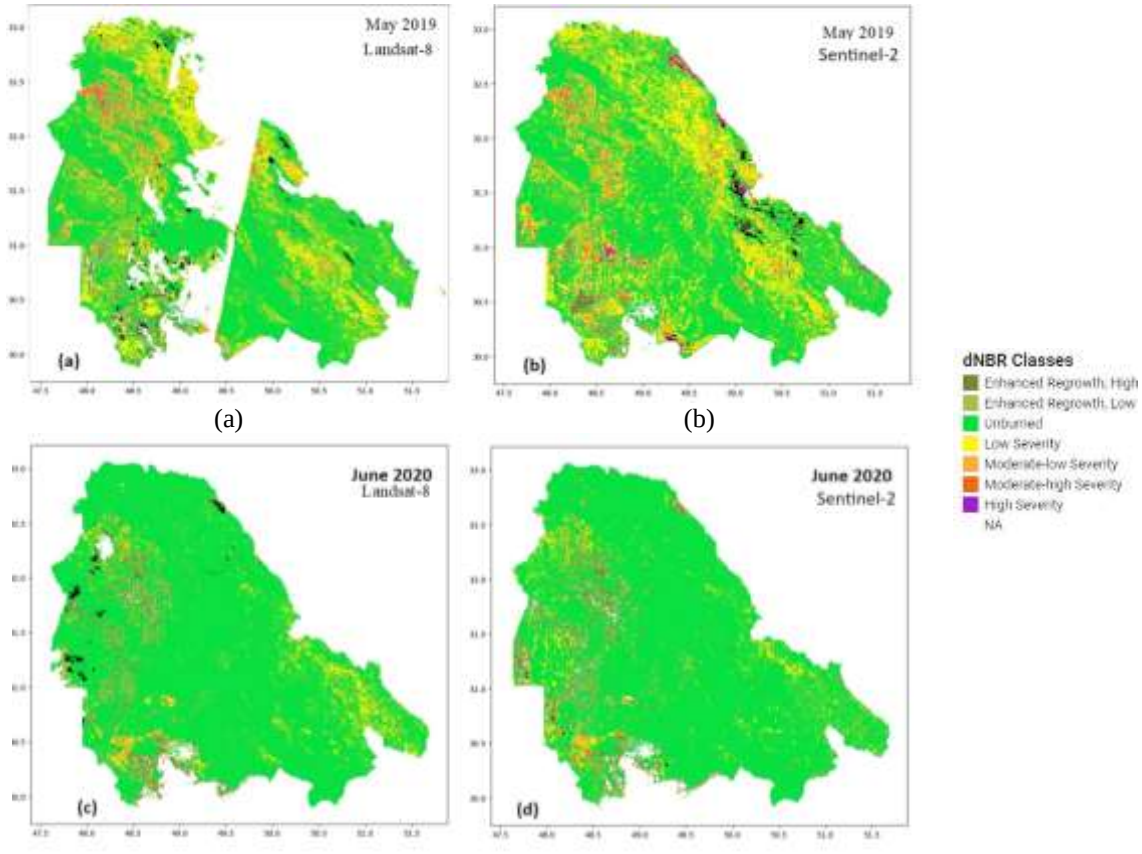

(a) (b)

(a) (b)

Figure 5. The effects of the forest fires that occurred in May 2019 and June 2020 within the study area, as depicted by burn severity maps derived from Landsat-8 (a, c) and Sentinel-2 (b, d) satellite imagery

Table 2 compares the burned areas detected by Landsat-8 and Sentinel-2 for the May 2019 event. In both cases, unburned areas represent the majority, covering more than 60% of the total mapped area. Landsat-8 identified a slightly lower total burned area (36.62%) compared to Sentinel-2 (39.52%). For both sensors, the "Low Severity" class is the most prevalent among burned areas. However, differences are observed between the two sensors across all severity classes, with Sentinel-2 consistently detecting larger burned areas in each category.

Table 3 presents a similar comparison for the June 2020 wildfire. Landsat-8 estimated a total burned area of 6,714.02 hectares (7.35%), whereas Sentinel-2 reported 6,067.88 hectares (6.46%). In this case as well, unburned zones dominate, comprising over 83% of the total area in both datasets. Although Landsat-8 recorded a slightly larger total burned area than Sentinel-2, differences persist across severity levels. Sentinel-2 detected more burned area in all severity categories except for "High Severity". These observed differences in burned area estimates between Landsat-8 and Sentinel-2 are largely explained by differences in spatial resolution and sensor characteristics. Sentinel-2, with a finer resolution of 10 meters, is capable of detecting smaller and more fragmented burn scars, especially in heterogeneous landscapes. This higher granularity enhances its ability to delineate fire perimeters more accurately, often resulting in higher total burned area estimates. For example, in the May 2019 event, Sentinel-2 detected approximately 36,135.63 hectares of burned area, while Landsat-8 recorded around 26,920.35 hectares—highlighting a difference of more than 9,000 hectares. A similar trend was observed in the June 2020 wildfire case, where Sentinel-2 consistently reported larger burned extents in most severity categories. These differences underscore the importance of sensor resolution in fire severity assessments. The slight discrepancies between the two datasets may be attributed to several factors. First, the coarser spatial resolution of Landsat-8 (30 meters) compared to Sentinel-2 (10 meters) could lead to under-detection of smaller burn scars, possibly inflating Sentinel-2's burned area estimates. Additionally, spectral differences between the sensors and the presence of missing or lower-quality data, particularly for Landsat-8—could further contribute to inconsistencies in the results (Guehaz and Sivakumar, 2023).

Table 2. Comparison of the burned area measured by Landsat-8 and Sentinel-2 satellites during the May 2019 wildfire event.

Class	Landsat-8			Sentinel-2		
	Hectares	Percentage	Pixels	Hectares	Percentage	Pixels
High Severity	75.69	0.1	841	496.98	0.54	5522
Moderate-high Severity	774.54	1.05	8606	1554.12	1.7	17268
Moderate-low Severity	3236.49	4.4	35961	4518.9	4.94	50210
Low Severity	18520.11	25.2	205779	24680.61	26.99	274229
Unburned	46580.31	63.37	517559	55303.56	60.48	614484
Enhanced Regrowth, Low	2589.66	3.52	28774	2710.53	2.96	30117
Enhanced Regrowth, High	1723.86	2.35	19154	2174.49	2.38	24161

Table 3. Comparison of the burned area measured by Landsat-8 and Sentinel-2 satellites during the June 2020 wildfire event.

Class	Landsat-8			Sentinel-2		
	Hectares	Percentage	Pixels	Hectares	Percentage	Pixels
High Severity	2.43	0	27	27.72	0.03	308
Moderate-high Severity	118.89	0.13	1321	204.93	0.22	2277
Moderate-low Severity	795.51	0.87	8839	860.76	0.93	9564
Low Severity	5777.19	6.35	64191	4874.49	5.28	54161
Unburned	76960.8	84.63	855120	77436.27	83.88	860403
Enhanced Regrowth, Low	4061.79	4.47	45131	4736.97	5.13	52633
Enhanced Regrowth, High	3223.44	3.54	35816	4179.6	4.53	46440

While both Landsat-8 and Sentinel-2 effectively captured the spatial extent and severity of burned areas, differences in their spatial resolution likely contributed to variations in the estimated burn areas. Sentinel-2's finer resolution (10 m) allows for better detection of small and fragmented burn scars, especially in heterogeneous landscapes, which often leads to larger total burned area estimates compared to the coarser 30 m resolution of Landsat-8. These discrepancies may also be influenced by spectral response differences, atmospheric corrections, and cloud cover masking performance between sensors. Therefore, results should be interpreted with an understanding of sensor-specific limitations, and integrating data from both platforms can help reduce uncertainty in post-fire assessments.

3-4. Effects of Weather Conditions and Fire Indices on Forest Fires

To gain a more detailed understanding of the conditions leading to wildfires in the study area, four fire indices—FWI, FDI, BI, and KBDI—have been analyzed to assess the fire risk under varying meteorological conditions. Figures 6 and 7 present the four fire indices for the two studied events, indicating favorable conditions for the occurrence of fires in the Kohgiluyeh and Boyer-Ahmad and Khuzestan provinces. Table 4 categorizes the FDI values (source: https://gacc.nifc.gov/rmcc/predictive/fuels_fire-danger/drgloss.htm), showing that the FDI values during the study days ranged from 30–60, which correspond to "very high" to "severe" fire danger levels. Under specific meteorological conditions characterized by warm air masses and convective instability, afternoon convective clouds often lead to thunderstorms and precipitation events. These conditions are particularly prevalent in the absence of a significant mid-level trough and minimal pressure gradients. In such scenarios, thermodynamic processes dominate, playing a critical role in shaping convective rainfall patterns (Moustakis et al., 2020). This process begins with surface heating, causing near-surface air to warm and become buoyant. As this warm, moist air rises, it encounters cooler air at higher altitudes, leading to the formation of convective clouds. Without a mid-level trough to cap the vertical ascent of warm air, these convective clouds can grow vertically, facilitated by the release of latent heat during condensation. Furthermore, the relatively uniform distribution of temperature and moisture in the absence of significant pressure gradients allows for more efficient convective processes. This means warm, moist air parcels can ascend freely, resulting in rapid development and intensification of convective clouds. Consequently, thunderstorms are more likely to occur during the afternoon when surface heating is at its peak, accompanied by lightning and rainfall (Xu, 2013). According to FIRMS data (Figure 8) and comparisons with Figures 6 and 7, fires occurred in the forests and pastures of the southern Zagros region. During both studied events (June 6–7, 2019, and May 20–21, 2020), fires in the southern Zagros forests coincided with cloudy conditions and afternoon rainfall. However, this rainfall primarily occurred over the Alborz and Zagros Mountain ranges. In other areas of the southern Zagros forests and pastures, either no rainfall occurred, or the amount was negligible. A synoptic analysis of atmospheric conditions (data not shown) during these two fire events revealed that high and extremely dry low-level air (relative humidity < 15%) prevailed when precipitation occurred, potentially evaporating before reaching the ground. Lightning struck during the peak afternoon heat (maximum daily air temperature). Convective instability associated with vertical motion, evidenced by negative omega values (figures not shown), rather than dynamic instability, contributed to the precipitation and cloudiness. Surface wind vector analysis showed weak winds (<4 m/s) during both events (figures not shown). FIRMS data confirmed wildfires in the Zagros forested region, particularly in southwestern Iran, including Khuzestan, Kohgiluyeh and Boyer-Ahmad provinces (Figure 6). Concurrent lightning activity during the study period was confirmed using data from the ENTLN, which provided cloud-to-ground strike records synchronized with fire detections. Consequently, thunderstorms with minimal or no precipitation, accompanied by dry lightning (data not shown), occurred in the southern Zagros region. Under favorable conditions,

such as the presence of dry leaves and vegetation and the occurrence of lightning, fires ignited in the study area. Fire indices, including FWI, FDI, BI, KBDI, and FIRMS data, remain critical for analyzing and understanding forest fires and their relationship with lightning in the southern Zagros region.

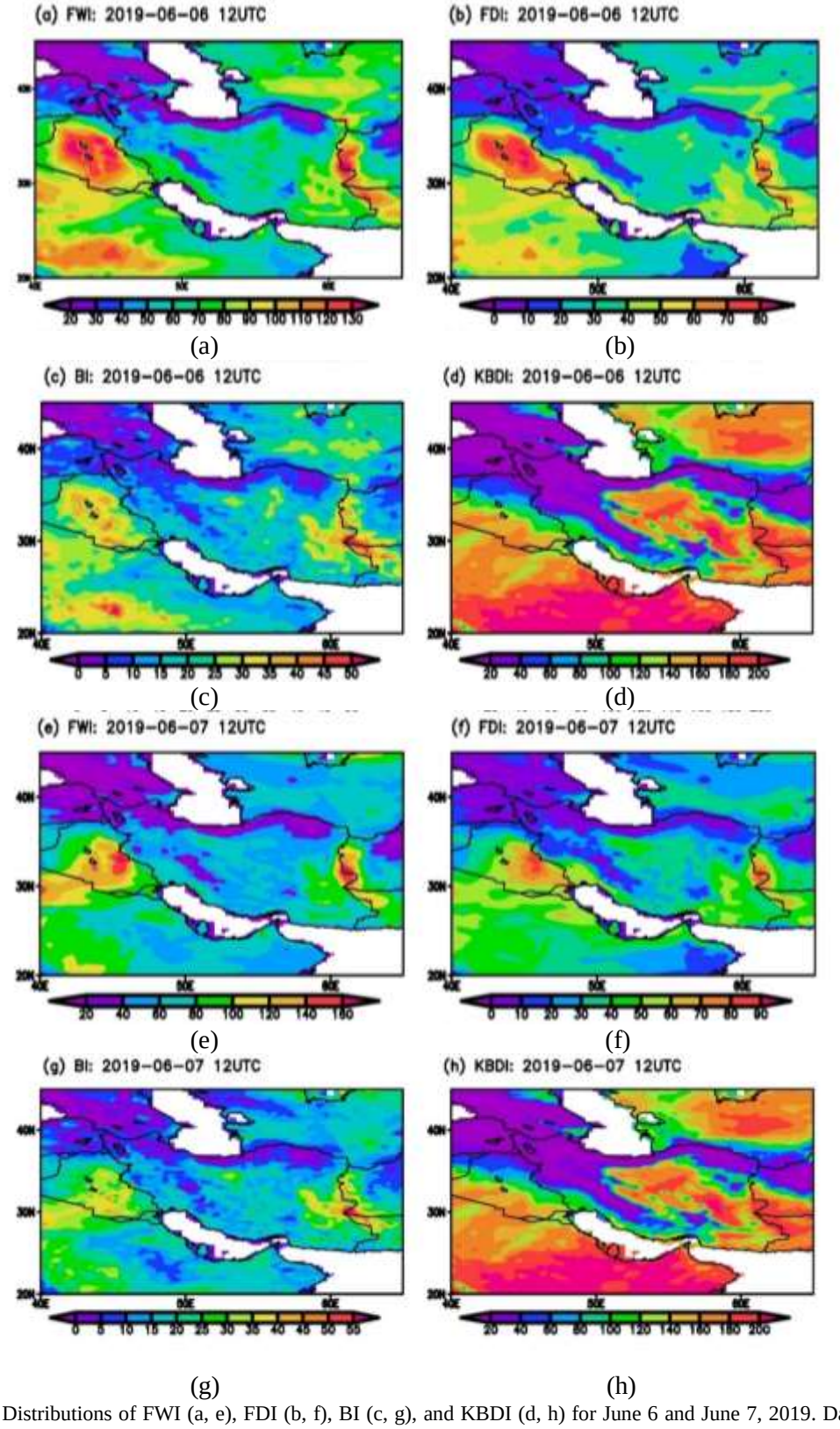

Figure 6. Distributions of FWI (a, e), FDI (b, f), BI (c, g), and KBDI (d, h) for June 6 and June 7, 2019. Data obtained from the ERA5 reanalysis dataset.

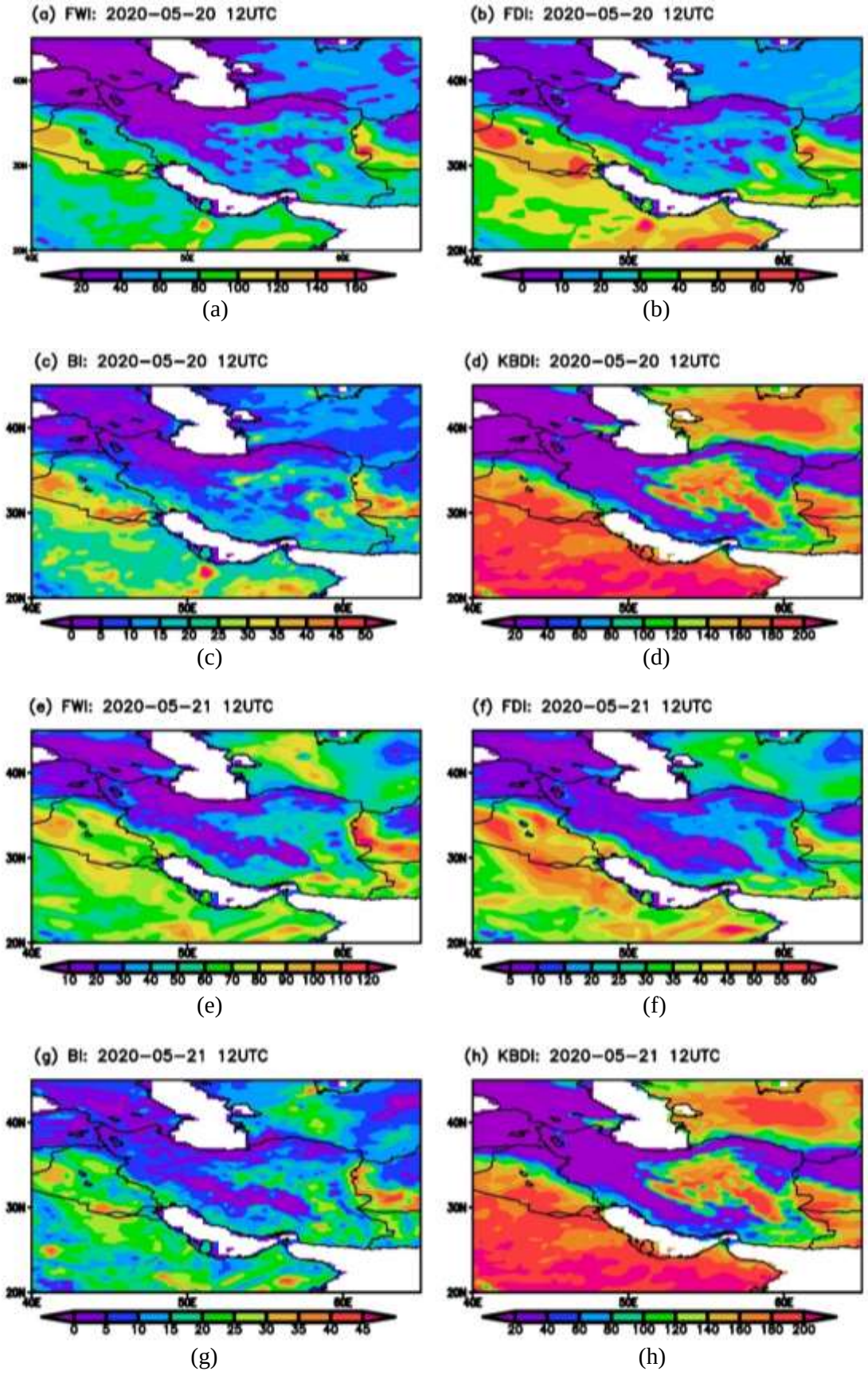

Figure 7. Distributions of FWI (a, e), FDI (b, f), BI (c, g), and KBDI (d, h) for May 20 and May 21, 2020. Data obtained from the ERA5 reanalysis dataset.

Table 4. Fire Danger Index (FDI) values and their corresponding fire danger levels.

Category	Forest Fire Danger Index
Catastrophic	100+
Extreme	75-99
Severe	50-74
Very high	25-49
High	12-24
Low-Moderate	0-11

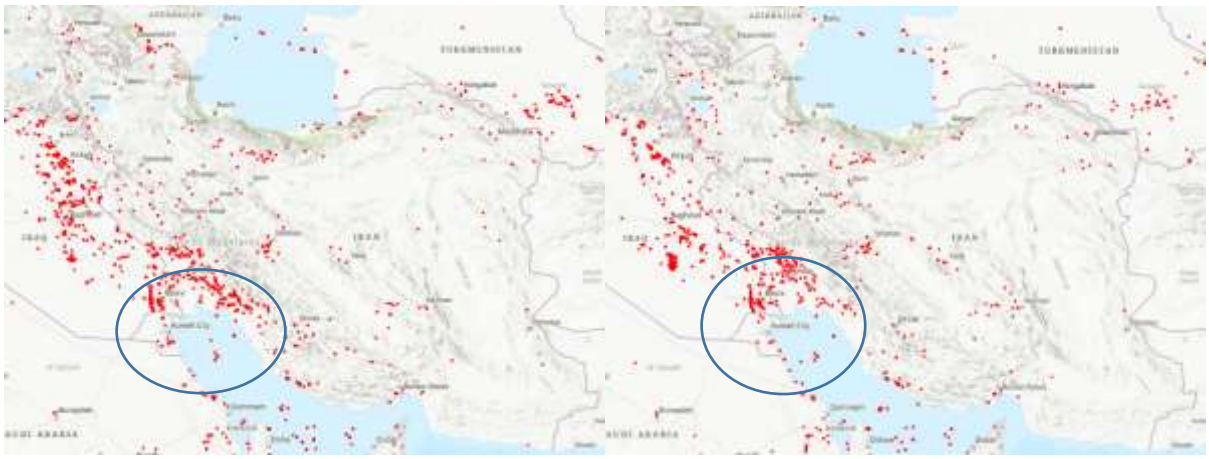

(a) (b)

Figure 8. Spatial distribution of VIIRS-detected forest fires (red dots) in Iran on June 6-7, 2019 (a) and May 20-21, 2020 (b). Data obtained from FIRMS.

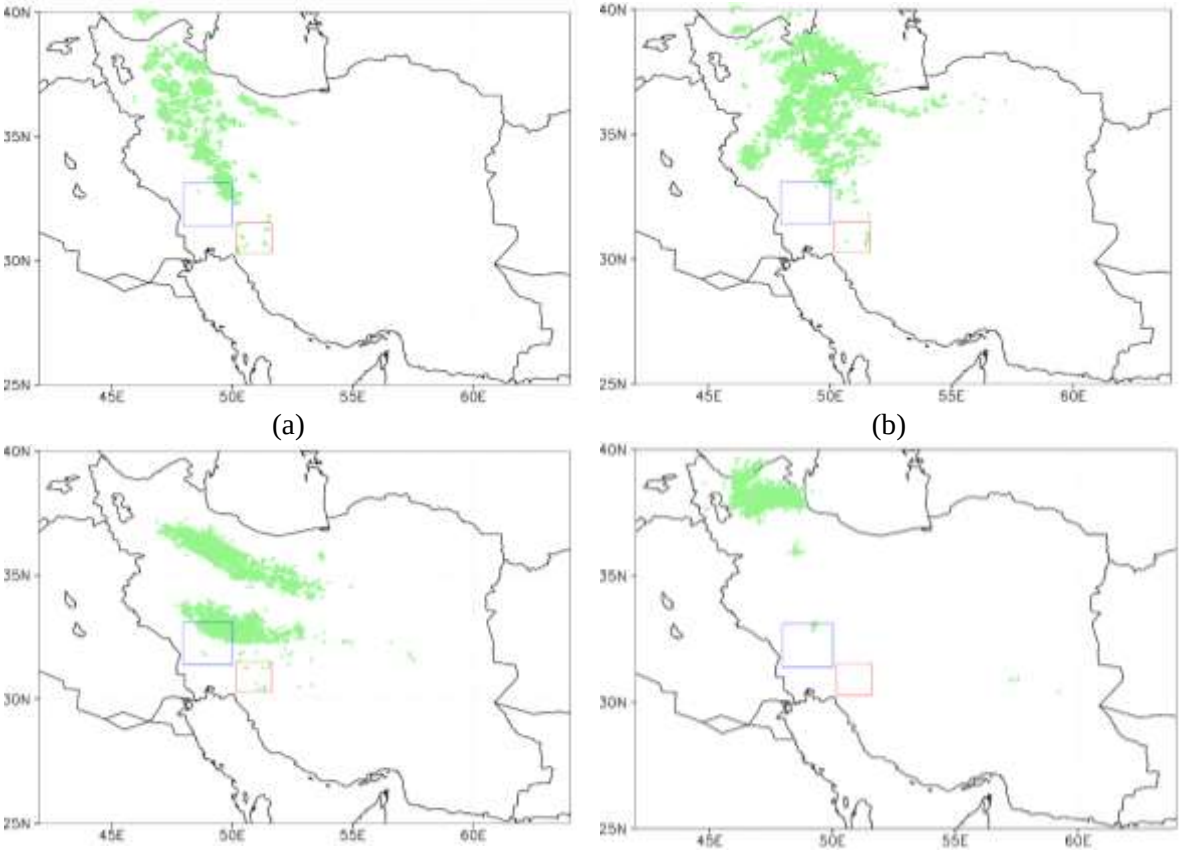

(a) (b)

(c) (d)

Figure 9. Locations of lightning (CG) occurrences on June 6 (a)–7 (b), 2019, and May 20 (c)–21 (d), 2020, obtained from the ENTLN.

3-5. Synergistic Role of Dry Lightning and FWI in Wildfire Ignition

To further validate the relationship between lightning activity and fire ignition potential, a spatiotemporal analysis was conducted for the two major wildfire events studied: June 2019 and May 2020. This analysis incorporated three key variables: (1) the number of dry lightning events, defined as lightning strikes occurring under conditions where the Fire Weather Index (FWI) exceeded 30, (2) daily mean FWI values, and (3) the number of confirmed high-confidence wildfires (confidence level = "h") based on VIIRS data.

The bubble charts (Figures 10 and 11) display these variables simultaneously. Each figure plots the daily timeline on the x-axis and the corresponding mean daily FWI values on the y-axis. The size of each bubble represents the number of dry lightning events recorded per day, while the color intensity reflects the number of high-confidence fire detections. On June 6 and 7, 2019, the highest counts of dry lightning (4,332 and 4,833, respectively) occurred alongside elevated FWI values (33.82 and 39.36), and these days also recorded the highest number of wildfires (914 and 969, respectively) (Table 5). This concurrence highlights the compound risk of wildfire ignition under conditions of both high flammability and frequent lightning activity. Similarly, during the May 2020 event, the peak dry lightning activity occurred on May 20 and 21, with 3,562 and 5,773 events, respectively. Although the mean FWI values (19.43 and 24.28) were lower than in June 2019, the number of fire detections remained high (321 and 313), emphasizing that even moderately elevated FWI values, when combined with intense lightning activity, can lead to widespread fire outbreaks (Table 6). These observations support the hypothesis that dry lightning acts as a critical ignition trigger only when the flammability of vegetation is elevated, as indicated by high FWI values. The co-occurrence of these three conditions—atmospheric instability (lightning), fuel dryness (FWI), and confirmed fire detections—strengthens the reliability of this integrated approach to wildfire risk assessment.

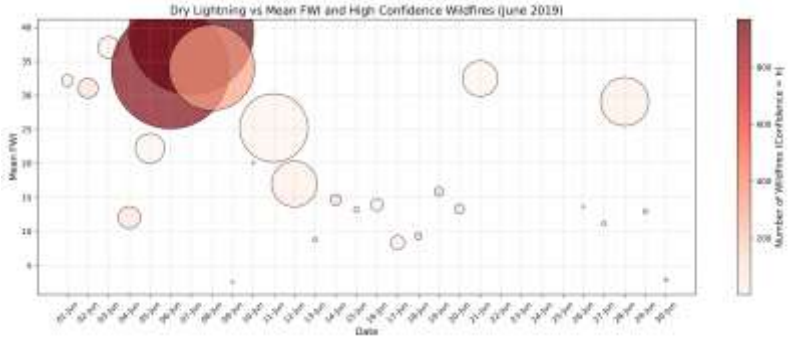

Figure 10. Bubble chart illustrating the combined daily occurrence of dry lightning, the Fire Weather Index (FWI), and high-confidence wildfires in the Zagros region during June 2019. The x-axis represents daily dates from June 1 to June 30. The y-axis shows the mean daily FWI values. Bubble size indicates the number of dry lightning events (FWI > 30) recorded each day, and bubble color intensity corresponds to the number of high-confidence wildfire detections ("h" category) from the VIIRS dataset.

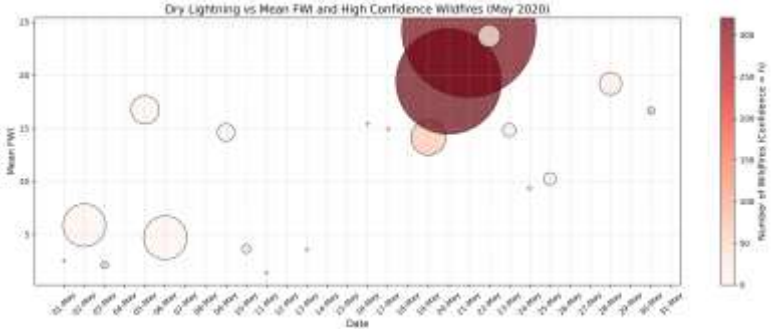

Figure 11. Bubble chart illustrating the combined daily occurrence of dry lightning, Fire Weather Index (FWI), and high-confidence wildfires in the Zagros region during May 2020. The x-axis represents daily dates from May 1 to May 31. The y-axis shows the mean daily FWI values. Bubble size indicates the number of dry lightning events (FWI > 30) recorded each day, and bubble color intensity corresponds to the number of high-confidence wildfire detections ("h" category) from the VIIRS dataset.

Table 5. Daily statistics of dry lightning, mean FWI, and wildfire detections (confidence = "h") for June 2019.

Date	Dry Lightning	Mean FWI	High-Confidence Wildfires
2019-06-07	4833	39.36	969
2019-06-06	4332	33.82	914
2019-06-08	2257	34.07	316
2019-06-25	36	15.22	188
2019-06-30	1	2.89	184

Table 6. Daily statistics of dry lightning, mean FWI, and wildfire detections (confidence = "h") for May 2020.

Date	Dry Lightning	Mean FWI	High-Confidence Wildfires
2020-05-20	3562	19.43	321
2020-05-21	5773	24.28	313
2020-05-19	395	14.13	69
2020-05-30	14	16.66	68
2020-05-03	14	2.12	63

4. Discussion and Conclusion

This study highlights the critical role of lightning as a primary trigger for wildfires in the Zagros Forest region of Iran, based on the analysis of events in June 2019 and May 2020. The findings corroborate with earlier research, such as the studies by Janssen et al. (2023), who also identified lightning as a significant factor in wildfire ignition under specific meteorological conditions. Analysis of FIRMS data confirmed wildfire occurrences in the southwestern provinces of Iran, particularly in Khuzestan, and Kohgiluyeh and Boyer-Ahmad. Furthermore, data from the ENTLN confirmed the presence of lightning activity during these fire events, which is consistent with previous studies (e.g., Song et al., 2024).

Under specific meteorological conditions—characterized by warm air masses, convective instability, and minimal pressure gradients—afternoon convective clouds frequently developed into dry thunderstorms that occurred without precipitation. These atmospheric conditions, exacerbated by the absence of a significant mid-level trough, amplified the wildfire risk. The study's use of fire indices such as the Fire Weather Index (FWI), Fire Danger Index (FDI), Burned Area Index (BI), and Keetch-Byram Drought Index (KBDI), alongside satellite data from Landsat-8 and Sentinel-2, provided valuable insights into the severity of the fires in May 2019 and June 2020. These indices have been similarly employed in other studies (e.g., Vicente-Serrano et al., 2010) to assess wildfire risks under varying climatic conditions.

The findings underscore the role of heavy rainfall in the previous year, which promoted vegetation growth, followed by rapid drying and warmer conditions that increased the wildfire risk. This sequence aligns with the work of Moustakis et al. (2020), who demonstrated how excess vegetation, when combined with subsequent drought, can contribute to wildfire susceptibility. Moreover, climate change, by exacerbating drought conditions, rising temperatures, altered precipitation patterns, and increased evaporation rates, significantly influences the frequency and severity of wildfires. This aligns with the findings of the IPCC (2018), which noted that climate change contributes to prolonged droughts, soil desiccation, and more intense atmospheric instability, all of which create favorable conditions for thunderstorms and wildfires.

To mitigate the impacts of climate change on thunderstorms and wildfires, a multifaceted approach is essential. This includes both mitigation and adaptation strategies. Key strategies to reduce the impacts of climate change and wildfire risks, as suggested by various studies (e.g., de Robinne et al., 2018), include: implementing sustainable land management practices to conserve soil moisture and reduce vulnerability to drought; developing robust early warning systems for detecting thunderstorms and wildfires, enabling timely responses and evacuations; promoting community-based initiatives such as forest fire prevention and suppression programs (including prescribed burns and fuel reduction); and transitioning to renewable energy sources to reduce greenhouse gas emissions and address the root causes of climate change.

Moreover, the quantitative validation conducted in this study confirms the compound role of dry lightning and elevated flammability conditions in triggering wildfires. In June 2019, the highest wildfire activity was observed on June 6 and 7, with 4332 and 4833 dry lightning strikes and corresponding FWI values of 33.8 and 39.4, respectively, accompanied by 914 and 969 high-confidence fire detections. A similar pattern was detected during May 2020, particularly on May 20 and 21, when 3562 and 5773 dry lightning strikes occurred, along with mean FWI values of 19.4 and 24.3. These days also recorded the highest wildfire activity in that month, with 321 and 313 high-confidence fire detections, respectively. These results reinforce the hypothesis that dry lightning alone is not sufficient to ignite fires unless coupled with favorable fuel and atmospheric conditions. The concurrent presence of dry lightning, elevated FWI values, and high fire counts on these peak days substantiates the synergy between atmospheric instability and fuel dryness in driving wildfire outbreaks.

However, it is important to emphasize that the conclusions drawn from this study are based solely on two specific case studies (June 2019 and May 2020). While these events provide compelling evidence of the interaction between dry lightning and fire-prone conditions in the Zagros region, they may not capture the full variability of wildfire behavior across different climatic years, regions, or ignition scenarios. Broader multi-year and multi-region analyses are therefore needed to assess the generalizability of these findings and to strengthen our understanding of lightning-induced wildfire dynamics under evolving climate conditions.

The combined effects of climate change, drought, and altered precipitation patterns significantly influence the occurrence of thunderstorms and increase the risk of wildfires. This study enhances our understanding of the wildfire dynamics in the Zagros region, emphasizing the importance of monitoring weather patterns, utilizing fire indices, and leveraging satellite data for effective wildfire management and mitigation. By understanding these complex interactions, policymakers and stakeholders can develop strategies to mitigate the impacts of climate change, strengthen ecosystem resilience, and protect vulnerable communities.

In addition to the key findings, this study provides operational insights for enhancing wildfire preparedness. We recommend that national and regional fire management systems incorporate lightning forecasting and monitoring tools, particularly during dry seasons, into their existing risk assessment frameworks. The integration of real-time lightning detection with fire weather indices (e.g., FWI > 30) can support early warning systems and help pre-position firefighting resources in lightning-prone zones.

However, this study also has several limitations. First, while the ENTLN lightning dataset offers high spatial and temporal resolution, its detection efficiency may vary across different terrains, particularly in mountainous regions like the Zagros. Second, the analysis was limited to two case studies that, although representative, do not allow for generalization across all of Iran. Lastly, differences in spatial resolution, revisit times, and atmospheric correction methods between Landsat-8 and Sentinel-2 may introduce uncertainties in burned area estimation. These limitations underscore the need for more extensive temporal and spatial studies combining field-based fire reports and high-resolution remote sensing datasets

Acknowledgments

The authors would like to express their gratitude to the European Centre for Medium-Range Weather Forecasts for providing the ERA-Interim data, as well as to NOAA/ESRL PSD, Physical Science Division, Boulder, Colorado, and the https://spei.csic.es/database.html website for providing SPEI data. Additionally, the observed lightning data include information obtained from the ENTLN, for which the authors extend their appreciation.

References

Barbero, R., Curt, T., Ganteaume, A., Maillé, E., Jappiot, M., & Bellet, A. (2018). Simulating the effects of weather and climate on large wildfires in France. https://doi.org/10.5194/nhess-2018-283

Bitar, A. A., Najem, S., Jarlan, L., Zribi, M., & Faour, G. (2021). Precipitation and soil moisture datasets show severe droughts in

the MENA region. doi:10.21203/rs.3.rs-141859/v1

Bowman, D. M., Williamson, G. J., Abatzoglou, J. T., Kolden, C. A., Cochrane, M. A., & Smith, A. M. (2017). Human exposure and sensitivity to globally extreme wildfire events. *Nature ecology & evolution*, 1(3), 0058.

Božiček, A., Đurović, M., Filipović-Grčić, B., Stipetić, N., & Franc, B. (2023). Impact of Lightning-Induced Wildfires on Power System Based on Satellite Data and Climatological Projections. In *New Energy and Future Energy Systems* (pp. 1-8). IOS Press.

Bryant, C. (2008). Deliberately lit vegetation fires in Australia. *Trends & Issues in Crime & Criminal Justice*, (350).

Bui, V. Y., Chang, L. C., & Heckman, S. (2015). A performance study of earth networks total lighting network (ENTLN) and worldwide lightning location network (WWLLN). In *2015 international conference on computational science and computational intelligence (CSCI)* (pp. 386-391). IEEE.

De Morais, J. C. M. (2013). Fighting Forest Fires in Brazil. In *International Symposium on Fire Economics, Planning, and Policy: Climate Change and Wildfires* (p. 179).

Di Giuseppe, F., Vitolo, C., Krzeminski, B., Barnard, C., Maciel, P., & San-Miguel, J. (2020). Fire Weather Index: the skill provided by the European Centre for Medium-Range Weather Forecasts ensemble prediction system. Natural Hazards and Earth System Sciences, 20(8), 2365-2378.

FAO. (2005). *Global Forest Resources Assessment 2005: Iran Country Report*. FRA 2005/082. Rome: Food and Agriculture Organization of the United Nations.

Fazel-Rastgar, F., & Sivakumar, V. (2022). Weather pattern associated with climate change during Canadian Arctic wildfires: A case study in July 2019. Remote Sensing Applications: Society and Environment, 25, 100698. http://doi:10.1016/j.rsase.2022.100698

Fazel-Rastgar, F. (2020). Extreme weather events related to climate change: widespread flooding in Iran, March–April 2019. SN Appl. Sci. 2, 2166 (2020). https://doi.org/10.1007/s42452-020-03964-9

Giglio, L., Randerson, J. T., & Van Der Werf, G. R. (2013). Analysis of daily, monthly, and annual burned area using the fourth-generation global fire emissions database (GFED4). *Journal of Geophysical Research: Biogeosciences*, 118(1), 317-328.

Gao, C., Shi, C., Li, J., Yuan, S., Huang, X., Zhang, Q., Wu, G. (2024). Igniting lightning, wildfire occurrence, and precipitation in the boreal forest of Northeast China. *Agricultural and Forest Meteorology*, 354, 110081. doi:10.1016/j.agrformet.2024.110081

Fuquay, D. M., Taylor, A. R., Hawe, R. G., & Schmid Jr, C. W. (1972). Lightning discharges that caused forest fires. *Journal of Geophysical Research*, 77(12), 2156-2158.

Guehaz, R., & Sivakumar, V. (2023). A case study about the forest fire occurred on 05 July 2021 over Khenchela province, Algeria, using space-borne remote sensing. *Frontiers in Remote Sensing*, *4*, 1289963.

Hersbach, H., Bell, B., Berrisford, P., Dahlgren, P., Horányi, A., Muñoz-Sabater, J., … Soci, C. (2020). The ERA5 global reanalysis: Achieving a detailed record of the climate and weather for the past 70 years. doi:10.5194/egusphere-egu2020-10375

IPCC. (2018). Special Report on Global Warming of 1.5°C.

Jaafari, A., Zenner, E. K., & Pham, B. T. (2018). Wildfire spatial pattern analysis in the Zagros mountains, Iran: A comparative study of decision tree based classifiers. *Ecological Informatics*, 43, 200-211. doi:10.1016/j.ecoinf.2017.12.006

Jaafari, A., Gholami, D. M., & Zenner, E. K. (2017). A Bayesian modeling of wildfire probability in the Zagros mountains, Iran. *Ecological Informatics*, 39, 32-44. https://doi.org/10.1016/j.ecoinf.2017.03.003

Jahdi, R., Salis, M., Darvishsefat, A. A., Mostafavi, M. A., Alcasena, F., Etemad, V., ... & Spano, D. (2015). Calibration of FARSITE simulator in northern Iranian forests. *Natural Hazards and Earth System Sciences*, 15(3), 443-459.

Janssen, T. A., Jones, M. W., Finney, D., van der Werf, G. R., van Wees, D., Xu, W., & Veraverbeke, S. (2023). Extratropical forests increasingly at risk due to lightning fires. *Nature Geoscience*, 16(12), 1136-1144.

Jiao, Q., Fan, M., Tao, J., Wang, W., Liu, D., & Wang, P. (2023). Forest Fire Patterns and Lightning-Caused Forest Fire Detection in Heilongjiang Province of China Using Satellite Data. *Fire*, 6(4), 166. https://doi.org/10.3390/fire6040166.

Kala, C. P. (2023). Environmental and socioeconomic impacts of forest fires: A call for multilateral cooperation and management interventions. *Natural Hazards Research*, 3(2), 286-294. doi:10.1016/j.nhres.2023.04.003

Kalnay, E., Kanamitsu, M., Kistler, R., Collins, W., Deaven, D., Gandin, L., ... & Joseph, D. (2018). The NCEP/NCAR 40-year reanalysis project. In *Renewable energy* (pp. Vol1_146-Vol1_194). Routledge.

Kalashnikov, D. A., Abatzoglou, J. T., Loikith, P. C., Nauslar, N. J., Bekris, Y., & Singh, D. (2023). Lightning-ignited wildfires in the western United States: Ignition precipitation and associated environmental conditions. *Geophysical Research Letters*, 50(16). doi:10.1029/2023gl103785

Keeley, J. E. (2009). Fire intensity, fire severity and burn severity: a brief review and suggested usage. *International journal of wildland fire*, 18(1), 116-126.

Key, C. H., & Benson, N. C. (2006). Landscape assessment (LA). *In: Lutes, Duncan C.; Keane, Robert E.; Caratti, John F.; Key, Carl H.; Benson, Nathan C.; Sutherland, Steve; Gangi, Larry J. 2006. FIREMON: Fire effects monitoring and inventory system. Gen. Tech. Rep. RMRS-GTR-164-CD. Fort Collins, CO: US Department of Agriculture, Forest Service, Rocky Mountain Research Station. p. LA-1-55, 164*.

Lapierre, J., Hoekzema, M., Stock, M., Merrill, C., & Thangaraj, S. C. (2019, June). Earth networks lightning network and dangerous thunderstorm alerts. In *2019 11th Asia-Pacific International Conference on Lightning (APL)* (pp. 1-5). IEEE.

Lee, M. B. (2005, December). Outbreak and spread of forest fire. In *symposium at Bukyoung University, Busan, Republic of Korea* (Vol. 14).

Markos, G., Aristotelis, P., Stefanos, B., & Nikolaos, I. (2023). Correlation between Weather Conditions and Burnt Areas in 25 Years of Forest Firefighting by the Fire Brigade. Environmental Sciences Proceedings, 26(1), 137.

Mohammadian Bishe, E., Norouzi, M., Afshin, H., & Farhanieh, B. (2023). A Case Study on the Effects of Weather Conditions on Forest Fire Propagation Parameters in the Malekroud Forest in Guilan, Iran. *Fire*, 6(7), 251.

Moris, J. V., ConFedera, M., Nisi, L., Bernardi, M., Cesti, G., & Pezzatti, G. B. (2020). Lightning-caused fires in the Alps: Identifying the igniting strokes. *Agricultural and Forest Meteorology*, 290, 107990.

Moustakis, Y., Onof, C. J., & Paschalis, A. (2020). Atmospheric convection, dynamics and topography shape the scaling pattern of hourly rainfall extremes with temperature globally. *Communications Earth & Environment*, 1(1), 11.

Paulo, A. A., Rosa, R. D., & Pereira, L. S. (2012). Climate trends and behavior of drought indices based on precipitation and evapotranspiration in Portugal. *Natural Hazards and Earth System Sciences*, 12(5), 1481-1491. doi:10.5194/nhess-12-1481-2012

Pereira, M. G., Parente, J., Amraoui, M., Oliveira, A., & Fernandes, P. M. (2020). The role of weather and climate conditions on extreme wildfires. In Extreme wildfire events and disasters (pp. 55-72). Elsevier.

Podschwit, H., Jolly, W., Alvarado, E., Markos, A., Verma, S., Barreto-Rivera, S., ... & Ponce-Vigo, B. (2023). Estimating the effects of meteorology and land cover on fire growth in Peru using a novel difference equation model. Natural Hazards and Earth System Sciences, 23(7), 2607-2624.

Podur, J., Martell, D. L., & Csillag, F. (2003). Spatial patterns of lightning-caused forest fires in Ontario, 1976–1998. *Ecological modelling*, 164(1), 1-20.

Rahimi, I., Duarte, L., & Teodoro, A. C. (2024). Zagros grass index – a new

vegetation index to enhance fire fuel mapping: Case study in Zagros mountains. doi:10.20944/preprints202403.0453.v1

Rakov, V. A., Uman, M. A., Rambo, K. J., Fernandez, M. I., Fisher, R. J., Schnetzer, G. H., ... & Bondiou-Clergerie, A. (1998). New insights into lightning processes gained from triggered-lightning experiments in Florida and Alabama. *Journal of Geophysical Research: Atmospheres*, 103(D12), 14117-14130.

Rienecker, M. M., Suarez, M. J., Gelaro, R., Todling, R., Bacmeister, J., Liu, E., ... & Woollen, J. (2011). MERRA: NASA's modern-era retrospective analysis for research and applications. *Journal of climate*, 24(14), 3624-3648.

Robinne, F. N., Burns, J., Kant, P., Flannigan, M., Kleine, M., de Groot, B., & Wotton, D. M. (2018). Global fire challenges in a warming world. IUFRO.

Rorig, M. L., & Ferguson, S. A. (1999). Characteristics of lightning and wildland fire ignition in the Pacific Northwest. *Journal of Applied Meteorology*, 38(11), 1565-1575.

Rudlosky, S. D. (2015). Evaluating ENTLN performance relative to TRMM/LIS. *Journal of Operational Meteorology*, 3(2).

Sagheb-Talebi, K., Sajedi, T., & Pourhashemi, M. (2014). Forests of Iran: A Treasure from the Past, a Hope for the Future (No. 15325). Springer Netherlands.

Song, Y., Xu, C., Li, X., & Oppong, F. (2024). Lightning-induced wildfires: An overview. *Fire*, 7(3), 79. doi:10.3390/fire7030079

Thompson, K. B., Bateman, M. G., & Carey, L. D. (2014). A comparison of two ground-based lightning detection networks against the satellite-based Lightning Imaging Sensor (LIS). *Journal of Atmospheric and Oceanic Technology*, 31(10), 2191-2205.

Van Wagtendonk, J. W., Root, R. R., & Key, C. H. (2004). Comparison of AVIRIS and Landsat ETM+ detection capabilities for burn severity. *Remote sensing of environment*, 92(3), 397-408.

Vicente-Serrano, S. M., Beguería, S., & López-Moreno, J. I. (2010). A Multiscalar drought index sensitive to global warming: The standardized precipitation evapotranspiration index. *Journal of Climate*, 23(7), 1696-1718. doi:10.1175/2009jcli2909.1

Vitolo, C., Di Giuseppe, F., Barnard, C., Coughlan, R., San-Miguel-Ayanz, J., Libertá, G., & Krzeminski, B. (2020). ERA5-based global meteorological wildfire danger maps. *Scientific data*, 7(1), 216.

Williams, A. P., Abatzoglou, J. T., Gershunov, A., Guzman-Morales, J., Bishop, D. A., Balch, J. K., & Lettenmaier, D. P. (2019). Observed impacts of anthropogenic climate change on wildfire in California. *Earth's Future*, 7(8), 892-910.

Tehran Times. (2019). *Will Iran set all-time heat records this summer?* https://www.tehrantimes.com/news/435888/Will-Iran-set-all-time-heat-records-this-summer

Wotton, B. M., Nock, C. A., & Flannigan, M. D. (2010). Forest fire occurrence and climate change in Canada. *International Journal of Wildland Fire*, 19(3), 253-271.

Xu, W. (2013). Precipitation and convective characteristics of summer deep convection over East Asia observed by TRMM. *Monthly Weather Review*, 141(5), 1577-15

Zou, Q., Cui, X., Zhang, D. L., Zheng, D., & Chen, L. (2022). A statistical analysis of total lightning flashes and peak current from high-resolution ENTLN measurements in South China during 2017. *Journal of Applied Meteorology and Climatology*, 61(7), 780-799.